A Comparative Study of Health Monitoring Sensors based on Prognostic Performance

Hyung Jun Park[1], Nam Ho Kim[2], and Joo-Ho Choi[3]

[1]*Dept. of Smart Air Mobility, Korea Aerospace University, Goyang-si, Gyeonggi-do, 10540, Korea*
phj921029@kau.kr

[2]*Dept. of Mechanical and Aerospace Engineering, University of Florida, Gainesville, Florida, FL 32611, USA*
nkim@ufl.edu

[3]*School. of Aerospace & Mechanical Engineering, Korea Aerospace University, Goyang-si, Gyeonggi-do, 10540, Korea*
jhchoi@kau.ac.kr

ABSTRACT

In the safety critical systems such as industrial plants or aircraft, failure occurs inevitably during the operation, and it is important to prevent this while maintaining high availability. Therefore, a lot of efforts are being directed toward developing advanced prognostics algorithms and sensing techniques as an enabler for predictive maintenance. The key for reliable and accurate prediction not only relies on the prognostics algorithms but also based on the collection of sensor data. However, there is not much in-dept studies toward evaluating the varying sensing techniques based on the prediction performance and inspection scheduling. It would be more reasonable for practitioner to select different cost of sensors based on the sensors' contribution on reducing the cost on unnecessary inspection or measurement while maintaining its prognosis performance. Thus, the authors try to thoroughly evaluate the cost-effectiveness of the different sensor with respect to sensor resistance to noise. The simulation is conducted to analyze the prediction performance with varying measurement interval and different level of noise during degradation. Then real run-to-fail (RTF) dataset acquired from two different sensors are analyzed to design optimal measurement system for predictive maintenance.

1. INTRODUCTION

To prevent catastrophic event due to safety system failure, the Prognostics and Health Management (PHM) techniques have been thoroughly studied to monitor the system health status and enable preventive maintenance. One of the key enablers for reliable health monitoring is capturing and storing different kinds of data from various sensors that contain health condition information of the monitored equipment (Lei et al., 2018). From the measured data, practitioner can determine the current health condition using signal processing techniques, feature engineering, machine learning methods, etc. to further predict its remaining useful life (RUL) until failure based on various prognostics algorithms. The recent developments in sensing technology have provided numerous types of sensors to measure parameters such as acceleration, temperature, acoustic signals and etc. (Kalsoom et al., 2020). Acquiring high-quality information from various sensor types are more helpful for effective condition monitoring and prognostics. However, implementing great amount of sensors used in health monitoring research is impractical as it require a large amount of data storage and sensor implementation costs (Cheng, Azarian and Pecht, 2010). Therefore, a robust evaluation and guideline of each sensor capacity for health monitoring and prognostics need to be established.

The general method for sensor evaluation and selection is to select the degradation-relevant sensors which are adequate for prognostics. Liu et al (Liu et al., 2015) proposed entropy-based strategy to quantitatively select sensors that reflect the monotonic trend during degradation to perform engine health prognosis. Zhang et al (Zhang et al., 2020) and Coble et al (Coble and Hines, 2011) developed an additional selection metric considering the trend consistency of sensor data among different systems and validated with engine simulation datasets. The existing literatures for sensor selections are mainly focused on evaluating the sensors data to the degradation trend using metrics of monotonicity, correlation and robustness (Li et al., 2015; Zhang, Zhang and Xu, 2016; Liu et al., 2017; She and Jia, 2021). However, there is lack of sensor evaluation

toward actual prognosis performance with the applicability of prognostics algorithm. Moreover, most of the above studies aim to optimize the sensor network in case where a large amount sensor are installed and reduce the number of sensors for cost-effective prognosis. In this paper, authors focus more on analyzing and comparing typical sensors having different signal quality (level of noise interference) on prognosis performance and relate sensor costs on the effect of reducing amount of data during degradation.

Few studies have considered applicability of prognostics algorithms with the selection of different sensors. Camci et al (Camci et al., 2016) focused on developing guideline for practitioners on various types of sensors used to monitor the status of railway turnout system. The RUL performances of sensors have been evaluated and additional cost factors of sensors are considered to make an economic justification of the optimal sensor selection. Nevertheless, the metrics to evaluate prognosis performance is based on the true degradation information (Saxena et al., 2010; Yang et al., 2016) such as true End of Life (EOL), true degradation curve, the availability of historical run-to-fail data, etc. However, in practice, the degradation trend and noise differ by each sensor, and it is challenging to assess true information.

Motivated by the above issues, this paper evaluates the prognosis performance of sensors having different level of noise interference during degradation. In more detail, the most common and cost-effective contact type sensor, accelerometer (Lee et al., 2014) is considered as one. An acoustic non-contact sensor, microphone is considered as another since it is recently drawing attention as an alternative due to its advantage of low interference with external noises within the system (Park et al., 2021). For the performance evaluation, the authors utilize the metric that does not require true degradation information and validate its correlation with true information-based metric through numerical study. Finally, the prognosis performance under different amount of data (different data acquisition interval) during degradation is addressed to validate the cost of higher quality sensor.

2. METHODOLOGY

An overall framework of the study is described in Fig. 1. First, the design parameters related to sensor such as level of noise and data interval (data amount) are changed to generate various case of degradation datasets. Then, true information-based RUL performance and time window metric without true information are calculated from degradation datasets. Finally, correlation between two metrics are evaluated to validate the use of time window strategy and the capability to reduce data amount while maintaining prediction performance is verified. Finally, the time window metric is used in the bearing run-to-fail (RTF) datasets to evaluate the performance of two different quality

sensors and cost-effectiveness of high-quality sensor is analyzed.

2.1. Degradation simulation

In the simulation, the degradation function is assumed to follow an exponential function since various components such as battery and bearing degradation are widely known to degrade exponentially (An, Choi and Kim, 2013a; Kim et al., 2020; Lim et al., 2020). Thus, using degradation function defined as Eq. (1), data until 100 cycles are generated by changing two design parameters. Four different level of noise is added to the degradation dataset by uniform distribution and four data interval is used to vary data amount during degradation which is summarized in table 1.

$$y_j = e^{(bt_j)} + \sigma, b = 0.02 \qquad (1)$$

Table 1. Sensor design parameters

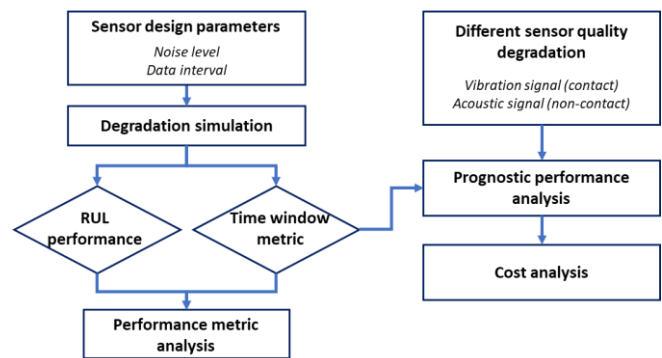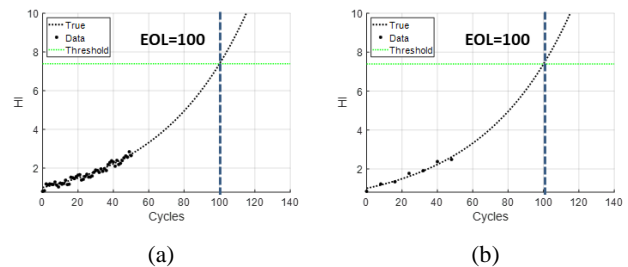| Lv. of noise	$\sigma \sim U(-Lv.noise, Lv.noise)$ $Lv.noise = [0.2, 0.3, 0.4, 0.5]$
Data interval	$\Delta t = t_j - t_{j-1}, \ \Delta t = [1, 2, 4, 8]$

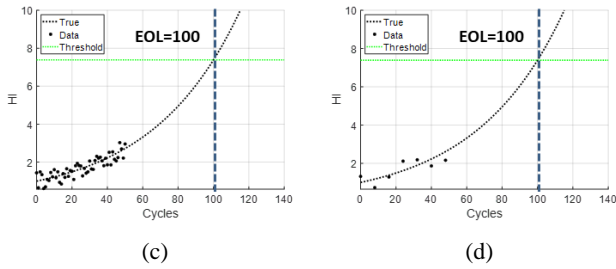Figure 1. Overall framework of sensor evaluation

(a)

(b)

(c) (d)

Figure 2. Degradation simulations

Based on the design parameters, total 16 cases are considered. The Fig. 2 (a) shows an example of dataset with small level of noise(0.2) and large amount of data($\Delta t = 1$). The black dots and dashed curved refer to measured data until 50 cycles and true degradation curve until end-of-life (EOL). A green line is the true threshold value at EOL which is used to calculate the predicted RUL. Fig. 2(b) is the case of small amount of data($\Delta t = 8$) and Fig. 2(c) and (d) are case under large level of noise(0.5). To consider the randomness of noise, 50 datasets are randomly generated under same design parameter.

2.2. Regularized Particle Filter (RPF)

Particle filter (PF) algorithm, also known as the Sequential Monte Carlo method is widely used prognostics approach in many engineering problems such as Lithium-ion batteries, induction motor and PEM fuel cells. PF recursively estimates and updates the probability distribution function (pdf) of the unknown model parameters or states of interest based on the following Bayes' theorem:

$$p(\theta|z) \propto L(z|\theta)p(\theta) \qquad (2)$$

where θ is a vector of unknown parameters, z is a vector of measurements, $L(z|\theta)$ is the likelihood, $p(\theta)$ is the prior pdf of θ and $p(\theta|z)$ is the posterior pdf of θ conditional on z. Standard PF consists of state transition function f to predict the evolution of the state and measurement function h as follows:

$$x_k = f(x_{k-1}, b_k, v_k) = exp(b_k dt)x_{k-1} \qquad (3)$$

$$z_k = h(x_k, n_k) \qquad (4)$$

where k is the time step index, x_k is the state, b_k is the vector of model parameter, z_k is the measurement data, and v_k and n_k are the process and measurement noises, respectively.

In this study, the exponential function is used for transition function and process noise is ignored since it can be handled through the uncertainty in the model parameters. For measurement, it is assumed that z_k is the same as degradation data including measurement noise having Gaussian noise, $n_k \sim N(0, \sigma_k)$, where σ_k is the unknown parameter estimated over time. Thus, the total unknown parameters to be estimated are $\theta = [x, b, \sigma]^T$.

The process of the PF is composed of three steps at each iteration. First, in prediction step, propagates the previous time step particles through state function to form particles at the current time, which is the prior pdf $p(\theta)$ at the current time. Then in the updating step, the likelihood of measurement data $L(z|\theta)$ that represents each particle's weight are calculated. As a new measurement is used, the weight of each particle is adjusted and assign a higher weight to the particles having a higher similarity with the measurement. Finally, in the resampling step, the particles are rearranged based on the obtained likelihood, which are duplicated or eliminated depending on the weight of the particles by using the inverse cumulative distribution function (CDF) method (Saha, Goebel and Christophersen, 2009; Dong et al., 2014). The resampled particles, which are the posterior distribution at the current time are then used as the initial distribution for the next step prediction. More information about PF is referred to (An, Choi and Kim, 2013b).

However, due to resampling process, PF-based prognosis suffers the problem of particle impoverishment since the samples are drawn from a discrete distribution rather than a continuous one. Consequently, after several iterations, the particles with small weights are discarded and the particles with high weights are duplicated too often which gives a poor representation of the posterior density. To resolve this issue, this study used regularized Particle filter (RPF) which is a modified version of PF in the resampling step. The kernels are generated at each particle points and summed to generate the kernel density estimate in RPF to have the advantage of approximating the weighted particles in continuous distributions (Musso, Oudjane and Legland, 2000).

2.3. Prognosis Performance Metric

After predicting the future degradation using the RPF algorithm, two different prognostic performance metrics are calculated: RUL performance metric and time window metric. To compare the performance of both metrics, two components are considered: the measure of the prediction accuracy and the measure of the uncertainty associated with the prediction. The schematic illustration of each metric calculation is addressed in Fig 3.

The RUL performance metric is calculated based on the result shown in the left figure of Fig. 3. The black dots and black dashed line represent the measured data until current cycle ($M = 50 cycles$) and true degradation curve respectively. Measurement data until M cycles are used for estimating the distribution of model parameters. The red dashed line and light red colored space denote the predicted median and 90% confidence interval (C.I.) in the future. The green dotted line horizontally is the true threshold until failure which is the value corresponding to EOL (100 cycles). Based on the threshold, we can obtain the distribution of cycles when the predicted state reaches the

threshold. Then the distribution of RUL can be obtained by subtracting this pdf from current cycle which is 50 cycles. From the predicted RUL distribution, the accuracy measure can be calculated by Eq (5) which is an absolute error between median value of predicted RUL and true RUL. Besides accurate prediction, the level of uncertainty associated with the prediction is also an important factor to assess the prognostics performance from a conservative decision-making point of view. Therefore, the level of uncertainty is considered as normalized C.I. width which is
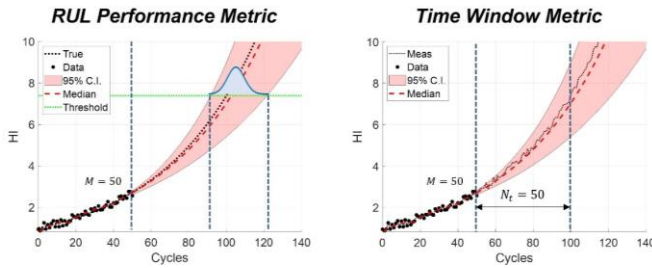

Figure 3. Illustration of two different prediction performance strategy

defined as RUL_{CI} and calculated by Eq. (6).

$$RUL_{error} = |RUL_{pred,median} - RUL_{true}| \qquad (5)$$

$$RUL_{CI} = \frac{RUL_{est,5^{th}} - RUL_{est,95^{th}}}{RUL_{true}} \qquad (6)$$

The time window metric is different from RUL metric as it directly uses the measurements in a certain time window without true information from degradation (Wang *et al.*, 2019). The strategy is shown in the right figure of Fig. 3 and the black dashed line is not a true degradation curve, but the measurement data. Since the true crack size is not available in practice, a straightforward way is to compare the predictions with data (Lei et al., 2018; Wang et al., 2019). Thus, the prediction accuracy and level of uncertainty are assessed over the time window which is the range between two vertical dashed line in the right figure. The length of time window (N_t) is set based on how much early prediction is required for maintenance scheduling. In the simulation study, the length of window is set 50 cycles same as the true RUL. The normalized mean square discrepancy (NMSD) is calculated to assess the prediction accuracy using below equation:

$$NMSD = \frac{1}{\max(y_{M+1:N_t}) - \min(y_{M+1:N_t})} MSD,$$

$$MSD = \frac{1}{N_t} \sum_{i=1}^{N_t} (y_{M+i} - \hat{x}^m_{M+i})^2 \qquad (7)$$

where M is the prediction start cycle, y is the measured data in the time window and $\hat{x}^m$ is the predicted median of degradation state by the prognostic algorithm.

For the uncertainty measure, two indexes are considered together. The first index E_1 measures the relative width of the 90% C.I. with respect to the predicted median value for each cycle and averages over the time window, which is defined by Eq. (8). Thus, a smaller E_1 indicates a narrower C.I. over prediction and lower prediction uncertainty.

$$E_1 = \frac{1}{N_t} \sum_{i=1}^{N_t} \frac{(\hat{x}^u_{M+i} - \hat{x}^l_{M+i})}{\hat{x}^m_{M+i}} \qquad (8)$$
, $\hat{x}^l$ & $\hat{x}^u$: Lower & upper bound of 90% C.I.

The second index E_2 measures whether the C.I. of prediction covers the true measurement and how wide the C.I. needs to be to cover the measurement at each prediction point. In detail, at each cycle in the time window, $M + i$, $i = 1,2, \ldots, N_t$, the minimal α% C.I. that can cover the measure is calculated. The discrete values of α is increased from 90 to 99 with one increment and E_2 is calculated as $-0.01\alpha + 1$. A smaller α indicates a more reliable prediction, thus a larger value is assigned for E_2. If the highest $\alpha = 99$ cannot cover the measurement, E_2 is defined zero.

$$E_2 = \begin{cases} \frac{1}{N_t} \sum_{i=1}^{N_t} -0.01\alpha_{M+i} + 1, \alpha = 90, 91, \ldots, 99 \\ 0, if\ required\ \alpha\ exceeds\ 99 \end{cases} \qquad (9)$$

The above two indexes evaluate the prognostics uncertainty considering the C.I. of prediction. Based on each index characteristic, the smaller the E_1 and higher the E_2 represents better prediction. Thus, nonlinear combination of E_1 and E_2, $EI = E_2/E_1$ is calculated as one index to assess uncertainty performance for time window metric.

2.4. Numerical Case Study

In this section, we attempt to evaluate the correlation between the RUL performance metric and the time window metric. Since the prediction performance of prognostic algorithm can differ by randomness of noise even under the same noise level, the correlation is analyzed using multiple randomly simulated datasets (50 datasets as mentioned before). If it has high correlation, the time window metric can be used to assess the true prediction performance using only measurement data.

The correlation is calculated between each component in metrics, the accuracy measure and uncertainty measure. The scatter plot and correlation coefficient value between two metrics under different level of noise are shown in Fig. 4. The upper figures present the scatter plot between RUL_{error} and NMSD and the lower figures between RUL_{CI} and EI.

Correlation between accuracy measures show very high correlation regardless of noise levels, smaller the RUL error, smaller the NMSD value. Though the uncertainty measure show less correlation than the accuracy measure, correlation coefficient value shows over 0.5 regardless of noise. Note that it has negative value since having higher EI value means more reliable prediction which corresponds to narrow RUL CI.

We verified that the time window metric has high correlation with true RUL performance and can be used as prediction performance indicator when true information is
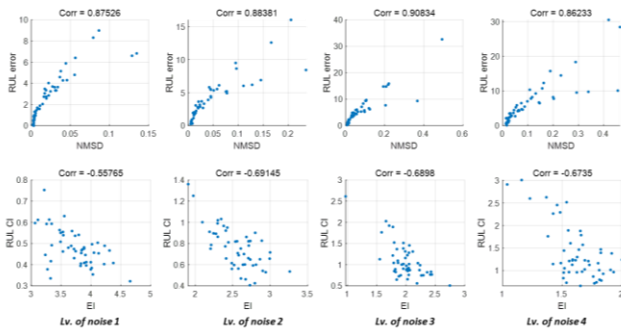

Figure 4. Correlation between two different metrics under varying noise
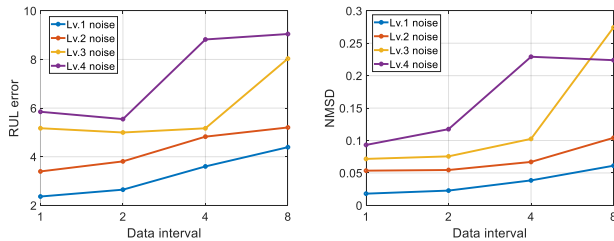

Figure 5. Prediction accuracy of dataset under varying level of noise with different data interval

unavailable. Moreover, the authors analyzed the prediction accuracy of dataset under varying level of noise with different data interval until current M cycles. Large data interval addresses small amount of data used for model parameter fitting. The overall result of RUL_{error} and NMSD are presented in Fig. 5 showing that measurement with small level of noise can have higher prediction accuracy than the measurement with larger noise while reducing the data amount. For example, the NMSD value at Lv. 1 noise & data interval of 4 cycles is smaller than the value at Lv. 3 noise & data interval of 1 cycle. Based on the verified hypothesis that metric without true information can assess the prediction performance and small level of noise data can maintain its performance higher than the high level of noise data, we evaluate the two different sensor data used on bearing health monitoring.

3. BEARING CASE STUDY

Bearing is one of the most critical components that leads to system failure and numerous researches have conducted to prevent its failure (Duong et al., 2018; Wang, 2018; Wu et al., 2019). Among the available sensors, the accelerometer has been the most common and cost-effective sensor for health monitoring. However, it has drawbacks of high interference with other signals due to its attachment within the system. Recently, acoustic non-contact sensor such as microphone are recently drawing attention as an alternative since it is less affected by the other signal interferences (Huang *et al.*, 2019; Wang, Mao and Li, 2021).
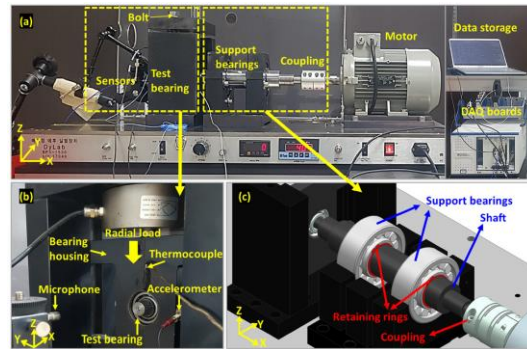

Figure 6. The bearing test rig: (a) Front view (b) Test bearing and sensors (c) Support bearings and couplings

To thoroughly evaluate the prognostics performance of two different quality sensors, the authors conducted multiple run-to-fail (RTF) experiment using a testbed mounted with commonly used accelerometer and high-quality microphone. The sensor performance regarding prognostics is evaluated using the time window metric from the previous section.

3.1. Experimental Setup

The Fig. 6 shows the bearing test rig in which the RTF tests are performed. The test rig consists of sensors, test bearings, support bearings, motor and DAQ boards. The sensors used in this study are an accelerometer (KS77C.100 by MMF) and a microphone (PCB Piezotronics 378C01) and a thermocouple. The cost of microphone (1931$) is about 4 times higher than the accelerometer (452$). The DAQ boards consist of NI Pxle-4464 and NI-9212, in which the former records acoustic and vibration signals at a sampling rate of 204.8 kHz and the latter records the temperature at a 100 Hz sampling rate. The first 1 second of every 10 seconds is stored as one cycle using LabVIEW software.

The bearing is tested under the shaft rotation at 1700 rpm. Radial load generated by the mechanical fastening of bolts is applied to the test bearing located at the end of the shaft at 75~80% of the dynamic load rating of 7950N to develop natural growing defects. After a number of trials to ensure the faults fully developed over cycles while maintaining

safety, the test is terminated when the acoustic pressure, acceleration and temperature exceed the thresholds of 9 Pascal, 18 m/s^2 and 80℃, simultaneously. In result, three RTF test datasets are acquired by two different sensor signals having different level of noise and pattern during degradation.

3.2. Sensor Performance Analysis

The general process of fault prognosis requires to extract a proper health indicator (HI) for the prognostics. In this study, a traditional time-based statistical feature, the root mean square (RMS) is calculated as HI since it is widely used for bearing degradation monitoring. Though, there are various
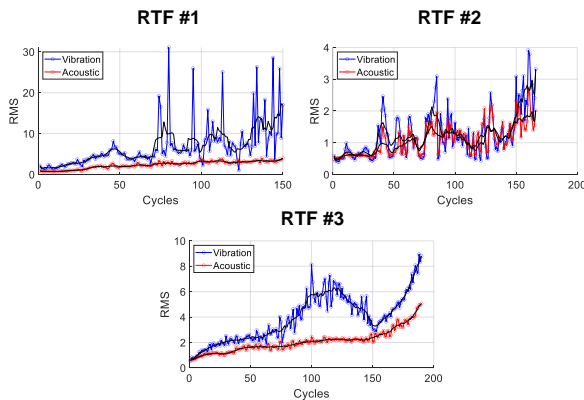

Figure 7. RMS values of three RTF datasets

studies that focused on developing robust HI for more accurate and earlier prediction, we use RMS since this article focuses more on evaluating the prognostics performance of different quality sensor data. The HIs for three different RTF datasets are presented in Fig. 7 where the blue and red dotted line is the HI from vibration signal and acoustic signal, respectively. It is noticeable that the vibration shows much fluctuation and noise interference compared to the acoustic signal. For the RTF #3, the HI from vibration shows not only large noise but also high fluctuation on the degradation trend itself.

The prognosis performance for each sensor is conducted using the time window metric. The window size (N_t) is fixed to 50 cycles in this study and prediction starting cycle (M) is 50 cycles which is used for PF model parameter fitting. Then the performance components representing the accuracy (NMSD) and uncertainty (EI) are calculated for every sequential cycle until failure. For example, the left and middle figures of Fig. 8 show the prediction result of RTF #1 dataset at each 50 cycles and 95 cycles, where upper figure is vibration and lower figure is acoustic. The black and red dots denote the measurement until current cycles and future measurement data in the time window. The red dashed line and light red colored space are the predicted median and 90% confidence interval (C.I.) in the

future. The NMSD and EI values over sequential cycle (from 50 cycles to 95 cycles) are shown at the right of Fig. 8 and averaged to evaluate the overall prognosis performance on each sensor data.

The prediction performance comparison of sensors for all RTF datasets are presented in Fig. 9. The upper histogram figures show the NMSD value, and the lower figures show the EI values related to uncertainty. The blue and red histogram are the prognosis metric results based on vibration and acoustic sensor, respectively. In addition, the results using data within interval of 4 cycles instead of 1 cycle are also compared together to evaluate the prognosis performance of acoustic sensor using less data amount. In the aspect of prediction accuracy, NMSD value of acoustic
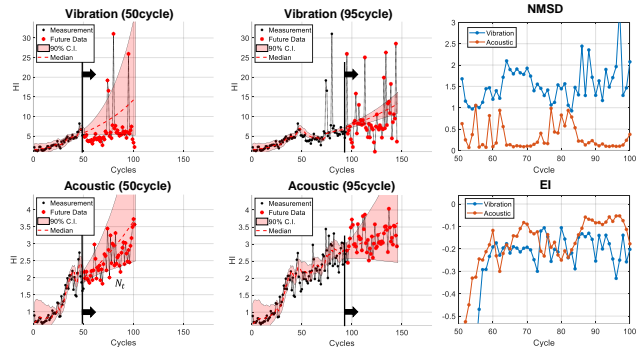

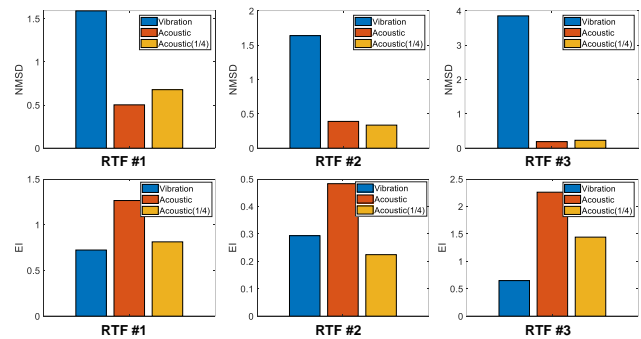Figure 8. Prediction trajectories for each sensor and prognosis performance over degradation

Figure 9. Prognosis performance comparison of vibration, acoustic and acoustic signal with less data (data interval of 4cycles)

is consistently lower than the vibration even if it uses 1/4 amount of data for model parameter fitting. The uncertainty measure EI shows that vibration sensor results lower reliability than the acoustic sensor over all RTF datasets. Though the acoustic EI values reduce when less data are used for the model parameter estimation, it is still similar or higher than the vibration. Thus, similar to the simulation study, the acoustic sensor, microphone having small level of noise during degradation perform much better prediction regardless of 1/4 times less data than the accelerometer.

Based on the prognosis performance comparison of two different sensor data, the effectiveness of microphone on prognostics is validated. Though the cost of microphone is higher than the conventional accelerometer, the performance on prediction accuracy and variation shows that microphone can provide much robust prediction even reducing the data storage costs. Considering the cost occurrence due to false prediction and data storage for long-term monitoring, the microphone will be cost-effective than implementing accelerometer.

4. CONCLUSION

A robust sensor performance comparison is proposed based on prognosis metric based only on direct measurement and without true degradation information. The validation of its metric is performance by randomly generating 50 datasets under different level of noise and calculating its correlation with true RUL performance. Then, addressed the advantage of using high quality sensor with less noise inference during degradation.

The bearing RTF experiments are conducted to demonstrate the two different quality sensors on prognosis performance. The non-contact sensor type, microphone showed superior performance on prognosis than the accelerometer due to the advantage of less interference to noise. Moreover, though the microphone costs much higher than the accelerometer, it is shown that it can reduce 4 times data amount than the accelerometer while maintaining its prognosis performance higher. This study is an initial step for setting a guideline for the practitioners when establishing the data acquisition system for PHM. The other factors such as calibration and regular maintenance of the instruments will be considered in the future work to evaluate sensor performance more robustly.

REFERENCES

An, D., Choi, J. H., & Kim, N. H. (2013a). Options for Prognostics Methods: A review of data-driven and physics-based prognostics. In 54th AIAA/ASME/ASCE/AHS/ASC *Structures, Structural Dynamics, and Materials Conference* (p. 1940).

An, D., Choi, J. H. and Kim, N. H. (2013b) 'Prognostics 101: A tutorial for particle filter-based prognostics algorithm using Matlab', *Reliability Engineering and System Safety*, 115, pp. 161–169. doi: 10.1016/j.ress.2013.02.019.

Camci, F. *et al.* (2016) 'Comparison of sensors and methodologies for effective prognostics on railway turnout systems', *Proceedings of the Institution of Mechanical Engineers, Part F: Journal of Rail and Rapid Transit*, 230(1), pp. 24–42. doi: 10.1177/0954409714525145.

Cheng, S., Azarian, M. H. and Pecht, M. G. (2010) 'Sensor systems for prognostics and health management', *Sensors*, 10(6), pp. 5774–5797. doi: 10.3390/s100605774.

Coble, J. and Hines, J. W. (2011) 'Applying the general path model to estimation of remaining useful life', *International Journal of Prognostics and Health Management*, 2(1), pp. 1–13.

Dong, H. *et al.* (2014) 'Lithium-ion battery state of health monitoring and remaining useful life prediction based on support vector regression-particle filter', *Journal of Power Sources*, 271, pp. 114–123. doi: 10.1016/j.jpowsour.2014.07.176.

Duong, B. P. *et al.* (2018) 'A Reliable Health Indicator for Fault Prognosis of Bearings'. doi: 10.3390/s18113740.

Huang, H. *et al.* (2019) 'Fault Diagnosis Accuracy Improvement Using Wayside Rectangular Microphone Array for Health Monitoring of Railway-Vehicle Wheel Bearing', *IEEE Access*, 7, pp. 87410–87424. doi: 10.1109/ACCESS.2019.2924832.

Kalsoom, T. *et al.* (2020) 'Advances in sensor technologies in the era of smart factory and industry 4.0', *Sensors (Switzerland)*, 20(23), pp. 1–22. doi: 10.3390/s20236783.

Huang, H. *et al.* (2019) 'Fault Diagnosis Accuracy Improvement Using Wayside Rectangular Microphone Array for Health Monitoring of Railway-Vehicle Wheel Bearing', *IEEE Access*, 7, pp. 87410–87424. doi: 10.1109/ACCESS.2019.2924832.

Kim, S. *et al.* (2020) 'A Novel Prognostics Approach using Shifting Kernel Particle Filter of Li-ion Batteries under State Changes', *IEEE Transactions on Industrial Electronics*, 0046(c), pp. 1–1. doi: 10.1109/tie.2020.2978688.

Lee, J. *et al.* (2014) 'Prognostics and health management design for rotary machinery systems - Reviews, methodology and applications', *Mechanical Systems and Signal Processing*, 42(1–2), pp. 314–334. doi: 10.1016/j.ymssp.2013.06.004

Lei, Y. et al. (2018) 'Machinery health prognostics: A systematic review from data acquisition to RUL prediction', Mechanical Systems and Signal Processing. doi: 10.1016/j.ymssp.2017.11.016.

Li, N. et al. (2015) 'An Improved Exponential Model for Predicting Remaining Useful Life of Rolling Element Bearings', IEEE Transactions on Industrial Electronics, 62(12), pp. 7762–7773. doi: 10.1109/TIE.2015.2455055.

Lim, C. et al. (2020) 'Feature extraction for bearing prognostics using weighted correlation of fault

frequencies over cycles', Structural Health Monitoring, p. 1475921719900917.

Liu, L. et al. (2015) 'Entropy-based sensor selection for condition monitoring and prognostics of aircraft engine', Microelectronics Reliability, 55(9–10), pp. 2092–2096. doi: 10.1016/j.microrel.2015.06.076.

Liu, L. et al. (2017) 'Quantitative selection of sensor data based on improved permutation entropy for system remaining useful life prediction', Microelectronics Reliability, 75, pp. 264–270. doi: 10.1016/j.microrel.2017.03.008.

Musso, C., Oudjane, N. and Legland, F. (2000) 'Improving Regularized Particle Filter', Sequential {M}onte-{C}arlo Method and Practice, (April), pp. 247–271.

Park, J. et al. (2021) 'Frequency energy shift method for bearing fault prognosis using microphone sensor', Mechanical Systems and Signal Processing. doi: 10.1016/j.ymssp.2020.107068.

Saha, B., Goebel, K. and Christophersen, J. (2009) 'Comparison of prognostic algorithms for estimating remaining useful life of batteries', Transactions of the Institute of Measurement and Control. doi: 10.1177/0142331208092030.

Saxena, A. et al. (2010) 'Metrics for Offline Evaluation of Prognostic Performance', International Journal of Prognostics and Health Management (IJPHM), 1(1), pp. 1–20.

She, D. and Jia, M. (2021) 'A BiGRU method for remaining useful life prediction of machinery', Measurement: Journal of the International Measurement Confederation, 167(3), pp. 1314–1326. doi: 10.1016/j.measurement.2020.108277.

Wang, D. (2018) 'Prognostics and Health Management : A Review of Vibration Based Bearing and Gear Health Indicators', IEEE Access, 6, pp. 665–676. doi: 10.1109/ACCESS.2017.2774261.

Wang, X., Mao, D. and Li, X. (2021) 'Bearing fault diagnosis based on vibro-acoustic data fusion and 1D-CNN network', Measurement: Journal of the International Measurement Confederation, 173(June 2020), p. 108518. doi: 10.1016/j.measurement.2020.108518.

Wang, Y. et al. (2019) 'Noise-dependent ranking of prognostics algorithms based on discrepancy without true damage information', Reliability Engineering and System Safety, 184(October 2017), pp. 86–100. doi: 10.1016/j.ress.2017.09.021.

Wu, J. et al. (2019) 'Degradation Data-Driven Time-To-Failure Prognostics Approach for Rolling Element Bearings in Electrical Machines', IEEE Transactions on Industrial Electronics, 66(1), pp. 529–539. doi: 10.1109/TIE.2018.2811366.

Yang, F. et al. (2016) 'Health index-based prognostics for remaining useful life predictions in electrical machines', IEEE Transactions on Industrial Electronics, 63(4), pp. 2633–2644. doi: 10.1109/TIE.2016.2515054.

Zhang, B. et al. (2020) 'Aircraft engine prognostics based on informative sensor selection and adaptive degradation modeling with functional principal component analysis', Sensors (Switzerland), 20(3). doi: 10.3390/s20030920.

Zhang, B., Zhang, L. and Xu, J. (2016) 'Degradation Feature Selection for Remaining Useful Life Prediction of Rolling Element Bearings', Quality and Reliability Engineering International, 32(2), pp. 547–554. doi: 10.1002/qre.1771.